Polymer Journal, Vol. 31, No. 6, pp 488—493 (1999)

Energy Transfer Study of Polymer Chain Morphology in a Two-Dimensional Monolayer

Nobuhiro SATO, Yousuke OSAWA, Shinzaburo ITO,† and Masahide YAMAMOTO

Department of Polymer Chemistry, Graduate School of Engineering, Kyoto University, Sakyo-ku, Kyoto 606-8501, Japan

(Received August 21, 1998)

ABSTRACT: The energy transfer method was utilized for evaluation of the two-dimensional chain morphology of poly(isobutyl methacrylate) in a deposited monolayer. A polymer labeled with phenanthrene as an energy donor and anthracene as an acceptor was diluted with unlabeled chains so that energy transfer occurring only within a single chain could be observed. As a result, from the fluorescence spectrum of the monolayer, the efficiency of the intrachain energy transfer was evaluated to be 19.2 (± 1.7)%. A computer simulation based on the Monte Carlo method was employed for the analysis of chain morphology. Various conformations of the model chains were generated by self-avoiding walk in the two-dimensional plane, and the statistical average value of energy transfer efficiency was obtained as a function of chain expansion. According to this relationship, the experimental efficiency corresponded to a radius of gyration of 6.2±0.8 nm. The morphological characteristics of the simulated chains suggest that the polymer chains take rather contracted forms and are segregated in two dimensions.

KEY WORDS Two-Dimensional Chain / Morphology / Energy Transfer Method / Polymer Monolayer / Segregation /

There have been numerous studies on monolayers at the air/water interface and Langmuir-Blodgett (LB) films aiming at constructing artificially-arranged molecular assemblies in a desired order.[1-3] Recently polymer LB films have widely been used instead of conventional LB films of fatty acids because of the advantages such as thermal and mechanical stability, thinness of each layer, and homogeneous dispersion of functional groups. In addition to the above applicational merits, polymer monolayers at the air/water interface attract scientific interest on their specific geometry of the molecular environment. Since the polymer chains in the monolayer are confined at the interface, their behavior is characteristic of two-dimensional systems and arouse our interest from a viewpoint of polymer science in two dimensions. Above all, the fundamental question is the conformation of polymer chains lying on the two-dimensional plane.

In his cerebrated book on polymer physics,[4] de Gennes presented a theoretical consideration for this as follows. On the one hand, when the segments of N units are connected with bonds of length a, the volume occupied by the single polymer chain in three-dimensional melts is of the order of $(N^{1/2}a)^3$, and the local concentration of the segments is $N/(N^{1/2}a)^3 = N^{-1/2}a^{-3}$. To build up the total concentration a^{-3}, the chains have to overlap one another. On the other, in two-dimensional melts, the local concentration is of the order of $N/(N^{1/2}a)^2 = a^{-2}$, same as the total concentration; consequently the chains are segregated.

We found recently from the molecular weight dependence of monolayer viscosity that there is little chain entanglement in the monolayer at the air/water interface up to relatively high molecular weights.[5] This result suggests that the two-dimensional chains are segregated.

Recent development of atomic force microscopy (AFM) enables direct observation of polymer chains in two dimensions. Kumaki *et al.* studied by AFM the morphology of polystyrene-*block*-poly(methyl methacrylate) (PS-*b*-PMMA) sparsely deposited onto a mica substrate, and excellently showed the morphology of the PMMA block chains extending over the substrate.[6] In spite of the obviousness of their result, it is likely to differ from the morphology of the chain in the monolayer because the PMMA block chain undergoes the rearrangement of its conformation influenced by the water adsorbed on the mica surface. Moreover, the chains surrounded by other chains probably have a conformation different from that of the isolated chains.

In this study, we took another approach to reveal the morphology of polymer chains in two dimensions by employing the fluorescence method. Excitation energy migration and transfer have been used for the evaluation of chain expansion in solutions and solids[7-9] because the rate of the transfer is highly sensitive to the chromophore–chromophore distance. It is therefore promising that this technique is also effectively applicable to the two-dimensional systems. By analyzing intrachain energy transfer rates, one can see whether the chains are contracted or expanded at the air/water interface.

To study the chain morphology by the energy transfer method, it is required that the chains labeled with fluorescent probes should be isolated enough from other labeled chains. To meet this requirement, the labeled chains must be diluted with unlabeled chains as much as possible. However, fluorescence emission from such dilute labeled chains in a monolayer is too weak to detect. Accordingly we prepared an LB film in which sufficiently distant two monolayers were deposited.

To evaluate chain expansion from the efficiency of the energy transfer, we need an appropriate function describing the morphology of the chain. Although a Gaussian distribution is applicable for three-dimen-

† To whom correspondence should be addressed (Tel: +81-75-753-5602, Fax: +81-75-753-5632, e-mail: sito@polym.kyoto-u.ac.jp).

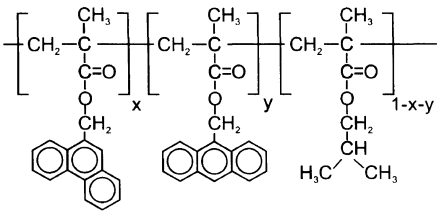

Figure 1. Chemical structure of the sample polymer labeled with fluorescent probes.

sional unperturbed chains in melts and concentrated solutions,[4] it is difficult to find well-defined expression for the chains confined in the two-dimensional systems. Thus, we employed a computer simulation to investigate the two-dimensional chain morphology.

EXPERIMENTAL

Materials

Figure 1 shows the structure of the sample polymer, poly(isobutyl methacrylate) (PiBMA), which was labeled with phenanthrene as an energy donor and anthracene as an energy acceptor. PiBMA is known to have a good transferability onto a solid substrate, and characteristics of PiBMA LB films are well investigated.[10] Since the glass transition temperature of PiBMA (*ca.* 53°C[11]) is sufficiently higher than the room temperature, molecular motion of the polymer backbone is frozen in the LB film.

The labeled PiBMA was synthesized by the radical copolymerization of isobutyl methacrylate, 9-phenanthrylmethyl methacrylate, and 9-anthrylmethyl methacrylate. Commercial isobutyl methacrylate (Nacalai Tesque) was used after distillation. The acceptor-containing monomer, 9-anthrylmethyl methacrylate, was synthesized by the esterification of methacryloyl chloride with 9-anthracenemethanol (Nacalai Tesque) in a tetrahydrofuran (THF) solution in the presence of pyridine and hydroquinone, and then recrystallized in methanol for purification. The donor-containing monomer, 9-phenanthrylmethyl methacrylate, was synthesized from 9-phenanthrenemethanol by the same procedure as the acceptor, but the purification was carried out by column chromatography on silica gel prior to the recrystallization. These three monomers were copolymerized in a benzene solution for 24 h at 60°C with α,α′-azobis(isobutyronitrile) (AIBN) as an initiator. The obtained polymer was purified by the reprecipitation from a benzene solution into methanol three times. The unlabeled PiBMA was also synthesized by the same procedure. Molecular weights were determined by GPC on the basis of calibration with polystyrene standards. For narrowing a molecular weight distribution, fractional precipitation was carried out in benzene/methanol solutions. As a result, the polydispersities, M_w/M_n, of the polymers were reduced to 1.4—1.5. The fractions of the donor and the acceptor were determined from the absorbance of the polymer in comparison with that of the low-molecular-weight model compounds, 9-phenanthrylmethyl trimethylacetate ($\varepsilon = 12100\,M^{-1}\,cm^{-1}$ at 298 nm in dichloromethane) and 9-anthrylmethyl trimethylacetate ($\varepsilon = 9300\,M^{-1}\,cm^{-1}$ at 368 nm in dichloromethane), which were synthesized from trimethylacetyl chloride by the same procedure as the fluorescent monomers. The results of the characterization are listed in Table I.

Table I. Characterization of the polymers

	x/%	y/%	$10^{-4}M_n$	M_w/M_n	DP[a]
Labeled PiBMA	7.2	0.41	7.81	1.41	512
Unlabeled PiBMA	0	0	3.98	1.51	280

[a] Number-average degree of polarization.

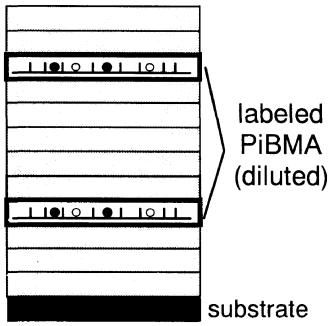

Figure 2. Layer structure of the LB film including monolayers of labeled PiBMA. Shadowed layers were made of unlabeled PiBMA for pre- and over-coating, and spacing.

Film Preparation

Monolayers at the air/water interface were prepared on a Teflon-coated aluminum trough. Benzene solutions (*ca.* $0.1\,g\,L^{-1}$ in concentration) of the labeled and the unlabeled polymers were mixed in a desired proportion and then dropped onto the surface of subphase water, which was in advance ion-exchanged, distilled, and then treated with a water purification system (Barnstead NANO Pure II). The subphase temperature was kept constant at 20°C by water circulation under the trough. After the monolayer was left for 20 min, it was compressed to a surface pressure of $10\,mN\,m^{-1}$, and then was deposited by the vertical dipping method at a rate of $15\,mm\,min^{-1}$ onto a hydrophobic quartz substrate, which was treated with trimethylchlorosilane prior to use. Macroscopic morphological feature was observed by Brewster angle microscopy, the apparatus for which is described elsewhere in detail.[12] As mentioned in the introductory section, two layers of the labeled PiBMA were deposited with a spacing of five layers. The layer structure is depicted in Figure 2. The unlabeled PiBMA was used for the precoating, spacing, and overcoating layers; thereby influence of the substrate and the quenching by atmospheric oxygen was reduced.

Fluorescence Measurement

Steady-state fluorescence spectra were measured with a fluorescence spectrophotometer (Hitachi model 850). A fluorescence decay was measured with the following single photon counting system. A Ti:sapphire laser system (Spectra Physics model 3950) was used for an excitation light source. Pulsed light from the laser was passed through a frequency tripler to have a wavelength

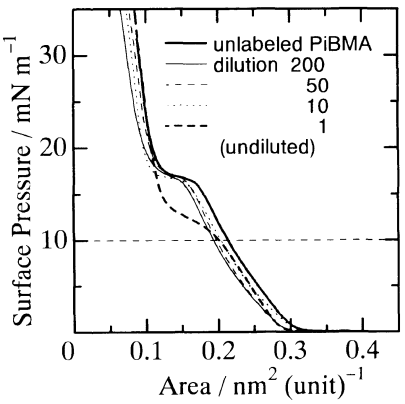

Figure 3. Surface pressure–area isotherms of the labeled PiBMA monolayers diluted with various fractions of unlabeled PiBMA.

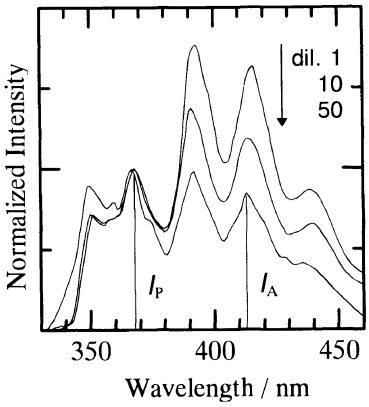

Figure 4. Emission spectra of the diluted monolayers. The intensity is normalized at 368 nm. As the dilution increases, relative intensity of anthracene (I_A) with respect to that of phenanthrene (I_P) decreases. See the text for details.

of 298 nm. Fluorescence emission from the sample was extracted with a monochromator, then detected by an end-on photomultiplier (Hamamatsu R3234). The total response function had an fwhm of 600 ps.

RESULTS AND DISCUSSION

Monolayer Property

Figure 3 shows surface pressure–area isotherms of PiBMA monolayers for various dilutions with the unlabeled PiBMA. Although the labeled PiBMA (undiluted) showed somewhat lower plateau pressure than the unlabeled one, all of the isotherms had a similar character as a condensed type monolayer. Actually, monolayers of dilutions above 10 showed identical profiles to that of the unlabeled polymer. According to a Brewster angle microscopy observation of the unlabeled PiBMA monolayer at the air/water interface, it was revealed that this monolayer has liquid-like character: fluid and deformable, as seen for acetalized poly(vinyl alcohol) monolayers.[12] Therefore it can be said that the PiBMA monolayer corresponds to a two-dimensional melt.

Fluorescence Measurement

As mentioned in the introductory section, the labeled polymer has to be diluted as much as possible, but thereby

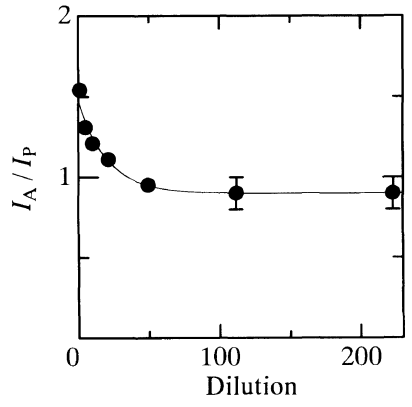

Figure 5. Dilution dependence of the energy transfer efficiency. The line shown in the figure is a guide for eyes.

observed fluorescence intensity becomes too weak to detect. Hence, we determined the adequate dilution by examining the dilution dependence of energy transfer efficiency. Figure 4 shows the steady-state fluorescence spectra obtained for monolayers of various dilutions. The samples were excited at 298 nm, where phenanthrene alone is selectively excited, and the spectra were normalized at 368 nm, where only the phenanthrene emission is observed. The relative intensity at *ca.* 412 nm, mainly due to the anthracene emission as a result of the energy transfer from phenanthrene, decreased to a constant as the dilution increased. This spectral change indicates that the interchain transfer was reduced and the energy transfer took place only within each isolated chain. The most dilute sample in Figure 4 showed a larger intensity at wavelengths around 350 nm. Because this emission could be ascribed to the emission of the unlabeled PiBMA, a contribution of the unlabeled PiBMA emission was subtracted from the measured spectra in the following calculation of an intensity ratio.

In this work, an intensity ratio, I_A/I_P, was used for a convenient measure of the transfer efficiency, where I_A and I_P denote the peak intensity of anthracene emission at *ca.* 412 nm and that of phenanthrene emission at *ca.* 368 nm, respectively. In fact, the intensity at *ca.* 412 nm contains a contribution of phenanthrene emission. For phenanthrene alone, intensity at *ca.* 412 nm was found to be 12% of that at 368 nm; accordingly it was subtracted from the total emission of the peak at *ca.* 412 nm. Influence of the anthracene excitation by the light of 298 nm was negligible because the absorbance at 298 nm was far smaller than those of phenanthrene. Figure 5 represents the dilution dependence of I_A/I_P. The value of I_A/I_P decreased with increasing dilution, indicating that the interchain energy transfer was reduced. At dilutions above 50, I_A/I_P reached a constant value: 0.88 ± 0.10. Thus, this value is due only to the intrachain energy transfer and contains information on the chain morphology in the two-dimensional plane.

As will be described in detail in the next section, the experimental value of I_A/I_P is compared with the results of the simulation. However the simulation yields the energy transfer efficiency in the expression of the quenching efficiency of the donor emission as follows.

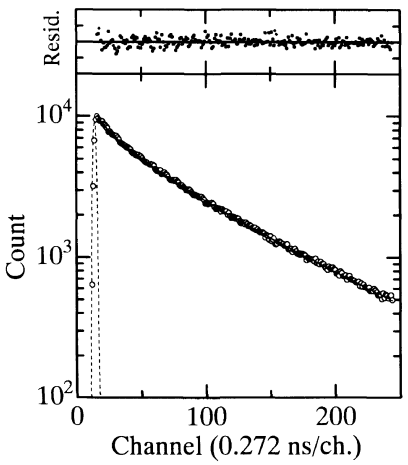

Figure 6. The fluorescence decay curve for a thick film of labeled PiBMA (undiluted).

$$E_T = 1 - \Phi/\Phi_0 \quad (1)$$

where E_T is the energy transfer efficiency, Φ and Φ_0 are the quantum yields of the donor fluorescence with and without acceptors, respectively. It is therefore necessary to know relationship between I_A/I_P and E_T to analyze the experimental result of the simulation.

Since I_A and I_P are proportional to E_T and $(1-E_T)$, respectively, the following equation holds.

$$E_T/(1-E_T) = \alpha(I_A/I_P) \quad (2)$$

where α is a constant. We determined the value of α by measuring a fluorescence decay of a PiBMA thick film showing sufficiently intense emission. If donors and acceptors are randomly distributed in a three-dimensional system where molecular motion is frozen and the orientation of the chromophores is isotropic, the decay function of donor fluorescence is expressed by the following equation.[13,14]

$$I(t) = \exp[-cA(t/\tau)^{1/2} - t/\tau] \quad (3)$$

with

$$c = \rho(4\pi R_0^3/3) \quad (4)$$

$$A = [(3/2)\kappa^2\pi]^{1/2} \quad (5)$$

where $I(t)$ is the normalized fluorescence intensity as a function of time t, c is the reduced concentration, τ is the intrinsic lifetime without the acceptors, ρ is the number density of the acceptors, R_0 is the Förster radius between the donor and the acceptor, and κ is the orientation factor, the value of which is 0.6901 in the current case.[14] The efficiency E_T is then given by

$$E_T = 1 - \int_0^\infty I(t)dt \Big/ \int_0^\infty e^{-t/\tau}dt \quad (6)$$

Since I_A/I_P is obtained independently from the steady-state fluorescence spectrum of the same film, α can be determined by eq 2. In experiment, we prepared a thick film (*ca.* 10 μm thick) of the labeled PiBMA (not diluted) by the solvent casting, and the fluorescence decay of the phenanthrene emission was measured. Figure 6 shows a decay curve for the PiBMA thick film. The curve was well fitted with eq 3, when the values for t and R_0 were 41.9 ns and 2.22 nm, respectively. Since the value of R_0 is appropriate for the phenanthrene–anthracene pair (*e.g.*, 2.172 nm was reported for a phenanthrene molecule and an anthracene molecule[15]), it can be said that the energy migration among the phenanthrene groups hardly occurred even in the three-dimensional film.

As a result of this experiment, α was determined to be 0.27. Hence, the limiting value of I_A/I_P, 0.88 ± 0.10, corresponds to $E_T = 19.2 \pm 1.7\%$.

Analysis by Simulation

To interpret the experimental result in association with the chain morphology, we employed a computer simulation based on the Monte Carlo method. As mentioned in the introductory section, morphology of three-dimensional unperturbed chains in melts or concentrated solutions is described by the Gaussian distribution and the statistical average of the energy transfer efficiency for such chains can be calculated theoretically. However, this is not the case for two-dimensional chains in melts.[4] For perturbed chains such as isolated chains in a dilute solution, the method of the self-avoiding walk has widely been employed to describe the chain morphology. We therefore used a model based on the self-avoiding walk for the two-dimensional chain. Because it is unlikely that the actual chain in a monolayer lies flat with all carbon atoms of its main chain locating exactly in the interfacial plane, some simplified model is preferred rather than an exact model for describing the two-dimensional chain. In the current study, we regarded a model chain as a series of freely-jointed floating monomer units and realized this chain on a two-dimensional hexagonal lattice. Then a segment of the model chain corresponds to one PiBMA monomer unit and the number of segments equals the degree of polymerization (DP). The effects of the bond angle, short-range steric restrictions, and cohesive interaction among side chains of actual chains are all included in the area of the monomer unit. A merit of this modeling is that the area occupied by one segment can be directly determined from the measurement of a surface pressure–area isotherm.

The procedure of the simulation is as follows. In the beginning, a model chain is extended on a two-dimensional hexagonal lattice, as shown in Figure 7. The area of the unit cell shown in this figure is given by the monolayer area at the deposition surface pressure. When the chain is lengthened by one segment from the current end, the destination site for the new segment is selected from the adjacent vacant sites in two manners. One is that the new site is randomly selected from the vacant sites (case A); the other is that it neighbors as many existing segments as possible (case B). For every site determination, either case is adopted with given probability. The probability for case B, hereinafter referred as the cohesion parameter, determines the chain expansion; namely, the chain becomes contracted when the cohesion parameter is close to unity. The cohesion parameter itself does not have any physical meaning, but it is a convenient variable to change the chain expansion in the simulation.

It is also necessary that the destination site is vacant. If all the adjacent sites are occupied, the current position

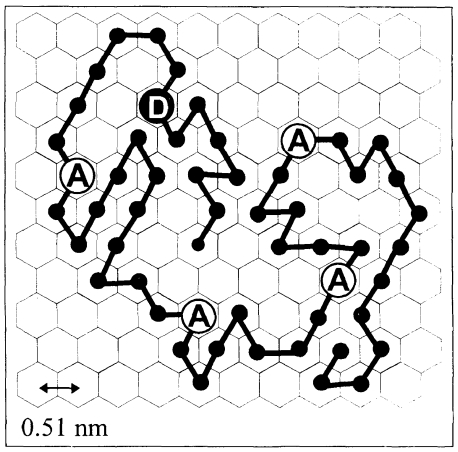

Figure 7. Model for the simulation. Chains are generated on a hexagonal lattice of a two-dimensional plane. Area of each cell is equivalent to that of the monomer units of the actual polymer.

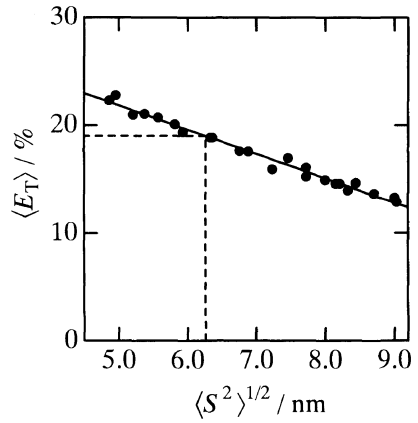

Figure 8. Relationship between statistically-averaged energy transfer efficiency and root-mean-square radius of gyration obtained for the simulated chains. The filled circles were obtained by the simulation and the solid line is drawn for a guide for eyes. The dashed line indicates the experimental value of E_T obtained by the fluorescence measurement and the corresponding radius of gyration.

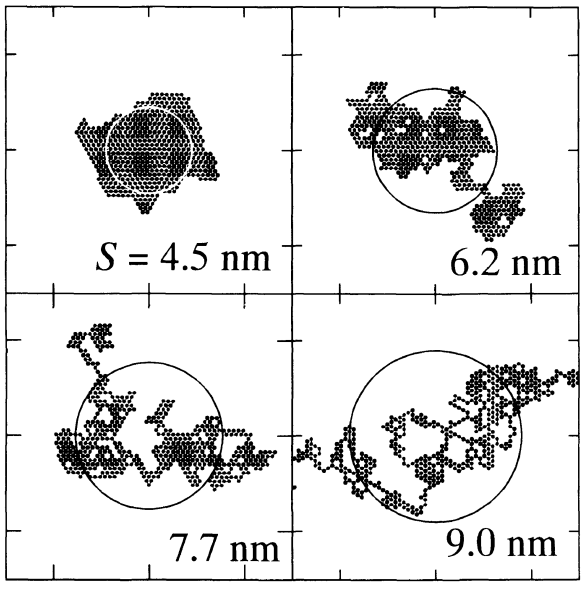

Figure 9. Typical morphology of the simulated chains. Each division of the axes is 10 nm. The radius of the circles in the figure represents the radius of gyration for each chain.

of the chain end is marked as a dead site and the chain end is shifted back to the previous site. Strictly speaking, it is statistically invalid to permit the reverse of the propagation end. Nevertheless, it is acceptable for the present study because the aim of this simulation is not to investigate the statistical mechanics of the chain conformation itself, but to obtain relationship between the energy transfer efficiency and a given chain conformation. It should be noted that the chain generated in this manner does not overlap with itself; therefore it is a kind of self-avoiding chains. When the chain length reached a desired value, the square radius of gyration, S^2, is calculated for the generated chain.

Next, the energy transfer efficiency is calculated. One donor and several acceptors are distributed on the generated chain. The donor is randomly placed on a segment of the chain. The acceptor positions are also randomly determined; however, the number of the acceptor, n_A, is not fixed but follows a binomial distribution $B(n,f)$, where n is the total number of segments (equivalent to DP) and f is the fraction of the acceptor unit. Then, the energy transfer efficiency is calculated as follows. The rate of the transfer k_i from the donor to acceptor i is given by

$$k_i = \tau^{-1}\left(\frac{R_0}{r_1}\right)^6 \tag{7}$$

where r_i is the distance from the donor to acceptor i. The total transfer rate, k_T, is obtained from the summation of k_i over all the acceptors.

$$k_T = \sum_{i=1}^{n_A} k_i \tag{8}$$

The decay function for a given conformation is then expressed by

$$I(t) = \exp[-(k_T + \tau^{-1})t] \tag{9}$$

Therefore the energy transfer efficiency E_T for a given conformation is obtained from eq 6 and 9 as below

$$E_T = 1 - \frac{1}{1 + k_T\tau} \tag{10}$$

Finally, the above calculation is repeated 5000 times for various conformations of chains and E_T and S^2 are statistically averaged for a given cohesion parameter. Thus we obtain the mean energy transfer efficiency $\langle E_T \rangle$ and the root mean-square radius of gyration, $\langle S^2 \rangle^{1/2}$. Varying the cohesion parameter from 0 to 1, relationship between $\langle E_T \rangle$ and $\langle S^2 \rangle^{1/2}$ can be obtained.

The cell area used for the simulation was 0.21 nm^2 determined from the average area of the diluted PiBMA monolayers at a surface pressure of 10 $mN\,m^{-1}$. The center-to-center distance between adjacent cells is calculated to be 0.51 nm. For DP and the fraction of the acceptor unit, the values listed in Table I were used. As a result of the simulation, variation of the cohesion parameter from 0 to 1 yields $\langle S^2 \rangle^{1/2}$ values ranging 9.0—4.5 nm.

Figure 8 shows the relationship between $\langle S^2 \rangle^{1/2}$ and $\langle E_T \rangle$. From this relationship, it is found that the experimental value of $\langle E_T \rangle$, $19.2 \pm 1.7\%$, corresponds to 6.2 ± 0.8 nm for $\langle S^2 \rangle^{1/2}$. However, the value of $\langle S^2 \rangle^{1/2}$

does not represent the morphology itself. To discuss the chain morphology from this $\langle S^2 \rangle^{1/2}$ value, we have to investigate the characteristics of simulated chains. Figure 9 displays typical morphologies of the simulated chains that give radii of gyration, S, of 4.5—9.0 nm. As seen for $S=4.5$ nm, a small value of S are resulted from a densely-packed chain, which keeps out the segments of other chains, indicating that chains are strongly segregated. On the other hand, as seen for $S=9.0$ nm, an extended chain has many indentations and voids which are supposed to be filled by the segments of other chains, indicating that chains penetrate into one another. The value of $\langle S^2 \rangle^{1/2}$ which was determined from the fluorescence measurement and the simulation was 6.2 ± 0.8 nm, thus it can be said that the polymer chain in the PiBMA monolayer took rather segregated forms.

Further discussion is needed on several points. First, effect of the chromophore orientation should be considered. The value of R_0 employed in the simulation was used as obtained from the decay measurement of the thick film, and no orientation effect was taken into account in the simulation. Therefore it may be expected that difference in the orientation factor between the two-dimensional film and the three-dimensional film led to incorrect estimation of the chain expansion. Nevertheless, the result obtained in the present study seems to be appropriate in view of an electronic property of phenanthrene. Even if the molecular orientation of phenanthrene is fixed, direction of its transition moment is not so definite because of low intrinsic anisotropy of phenanthrene fluorescence. Consequently the molecular orientation of phenanthrene is not very influential to the estimation of the chain expansion.

A question still remains whether the segregated two-dimensional chains observed in our study were in themodynamical equilibrium. Considering that the PiBMA monolayer was flexible and fluid at the air/water interface, and sufficient time was taken before compression of the monolayer, it is probable that the chains reached equilibrium. However, further investigation is necessary for verifying this.

CONCLUSION

To elucidate the polymer chain morphology in two dimensions, we applied the energy transfer method to a deposited monolayer of PiBMA labeled with phenanthrene and anthracene. Sufficient dilution of a labeled chain with unlabeled chains enables us to observe energy transfer within a single chain through the measurement of fluorescence spectra. From the intrachain energy transfer efficiency coupled with the computer simulation, it was revealed that the polymer chains are segregated in the two-dimensional monolayer system. To clarify the intrinsic nature of two-dimensional chain morphology unambiguously and quantitatively, examination of the polymers with different molecular weights cannot be avoided. Nevertheless, this work effectively shows a morphological characteristics of a polymer chain in a two-dimensional condensed medium which has been little known.

Acknowledgment. This work was supported by a Grant-in-Aid for Scientific Research (No. 09450360 and 10135216) from the Ministry of Education, Science, Sports and Culture of Japan.

REFERENCES

1. G. L. Gaines, Jr., "Insoluble Monolayers at Liquid-Gas Interfaces," Interscience, New York, N.Y., 1966.
2. H. Kuhn, D. Möbius, and H. Bücher, "Physical Methods of Chemistry," A. Weissberger and B. Rossiter, Ed., Wiley, New York, N.Y., 1972.
3. A. Ulman, "An Introduction to Ultrathin Organic Films from Langmuir–Blodgett to Self-Assembly," Academic, San Diego, California, 1991.
4. P. G. de Gennes, "Scaling Concepts in Polymer Physics," Cornell University, Ithaca, N.Y., 1979.
5. N. Sato, S. Ito, and M. Yamamoto, *Macromolecules*, **31**, 2673 (1998).
6. J. Kumaki, Y. Nishikawa, and T. Hashimoto, *J. Am. Chem. Soc.*, **118**, 3321 (1996).
7. K. A. Peterson, A. D. Stein, and M. D. Fayer, *Macromolecules*, **23**, 111 (1990).
8. G. Liu, J. E. Guillet, E. T. B. Al-Takrity, A. D. Jenkins, and D. R. M. Walton, *Macromolecules*, **23**, 1393 (1990).
9. G. Liu, J. E. Guillet, E. T. B. Al-Takrity, A. D. Jenkins, and D. R. M. Walton, *Macromolecules*, **24**, 68 (1991).
10. K. Naito, *J. Colloid Interface Sci.*, **131**, 218 (1989).
11. T. Hayashi, T. Okuyama, S. Ito, and M. Yamamoto, *Macromolecules*, **27**, 2270 (1994).
12. N. Sato, S. Ito, and M. Yamamoto, *Polym. J.*, **28**, 784 (1996).
13. Th. Förster, *Z. Naturforsch.*, **4a**, 321 (1949).
14. J. Baumann and M. D. Fayer, *J. Phys. Chem.*, **85**, 4087 (1986).
15. I. B. Berlman, "Energy Transfer Parameters of Aromatic Compounds," Academic, New York, N.Y., 1973.